High-throughput quantitation of serological ceramides/dihydroceramides by LC/MS/MS: Pregnancy baseline biomarkers and potential metabolic messengers

Qianyang Huang[a], Shiying Hao[b,c], Xiaoming Yao[a], Jin You[d], Xiao Li[a], Donghai Lai[a], Chunle Han[a], James Schilling[a], Kuo Yuan Hwa[a], Sheeno Thyparambil[a], John Whitin[e], Harvey J. Cohen[e], Henry Chubb[e], Scott R. Ceresnak[e], Doff B. McElhinney[b,c], Ronald J. Wong[e], Gary M. Shaw[e], David K. Stevenson[e], Karl G. Sylvester[d], Xuefeng B. Ling[c,d,*]

[a] mProbe Inc, Mountain View, CA, United States
[b] Department of Cardiothoracic Surgery, Stanford University School of Medicine, Stanford, CA, United States
[c] Clinical and Translational Research Program, Betty Irene Moore Children's Heart Center, Lucile Packard Children's Hospital, Palo Alto, CA, United States
[d] Department of Surgery, Stanford University School of Medicine, Stanford, CA, United States
[e] Department of Pediatrics, Stanford University School of Medicine, Stanford, CA, United States

ARTICLE INFO

ABSTRACT

Ceramides and dihydroceramides are sphingolipids that present in abundance at the cellular membrane of eukaryotes. Although their metabolic dysregulation has been implicated in many diseases, our knowledge about circulating ceramide changes during the pregnancy remains limited. In this study, we present the development and validation of a high-throughput liquid chromatography-tandem mass spectrometric method for simultaneous quantification of 16 ceramides and 10 dihydroceramides in human serum within 5 min. by using stable isotope-labeled ceramides as internal standards. This method employs a protein precipitation method for high throughput sample preparation, reverse phase isocratic elusion for chromatographic separation, and Multiple Reaction Monitoring for mass spectrometric detection. To qualify for clinical applications, our assay has been validated against the FDA guidelines for Lower Limit of Quantitation (1 nM), linearity (R^2>0.99), precision (imprecision<15 %), accuracy (inaccuracy<15 %), extraction recovery (>90 %), stability (>85 %), and carryover (<0.01 %). With enhanced sensitivity and specificity from this method, we have, for the first time, determined the serological levels of ceramides and dihydroceramides to reveal unique temporal gestational patterns. Our approach could have value in providing insights into disorders of pregnancy.

1. Introduction

Ceramides and dihydroceramides are subfamilies of sphingolipids characterized by the attachment of the aliphatic moieties onto the sphingosine and sphinganine backbones through amide-linkage. The inherent heterogeneity of the fatty acid molecules structurally diversifies both families of chemicals by conferring the individual species with a distinctive combination of carbon number and saturation degree on the aliphatic moiety (Fig. 1) [1]. Biosynthetically, ceramides are primarily generated by the de novo synthetic pathway from the endoplasmic reticulum via the collaborative actions of multiple enzymes in the presence of transiently produced intermediates. Among the transient intermediates, dihydroceramides are known as the immediate precursors that can be directly converted to ceramides via oxidation catalyzed by dihydroceramide desaturase [2]. Ceramides are present in abundance on the membrane of eukaryotic cells along with other integral membrane components, including trans-membrane proteins, sphingomyelins, cholesterols, and glycosphingolipids. These components collectively form characteristic regions known as glycolipid-enriched microdomains or lipid rafts on the eukaryotic cell membrane, which play fundamental roles in maintaining the integration and dynamic behavior of the lipid bilayer scaffold [3]. In addition to their importance for the structural folding of eukaryotic

* Corresponding author.
  E-mail address: bxling@stanford.edu (X.B. Ling).

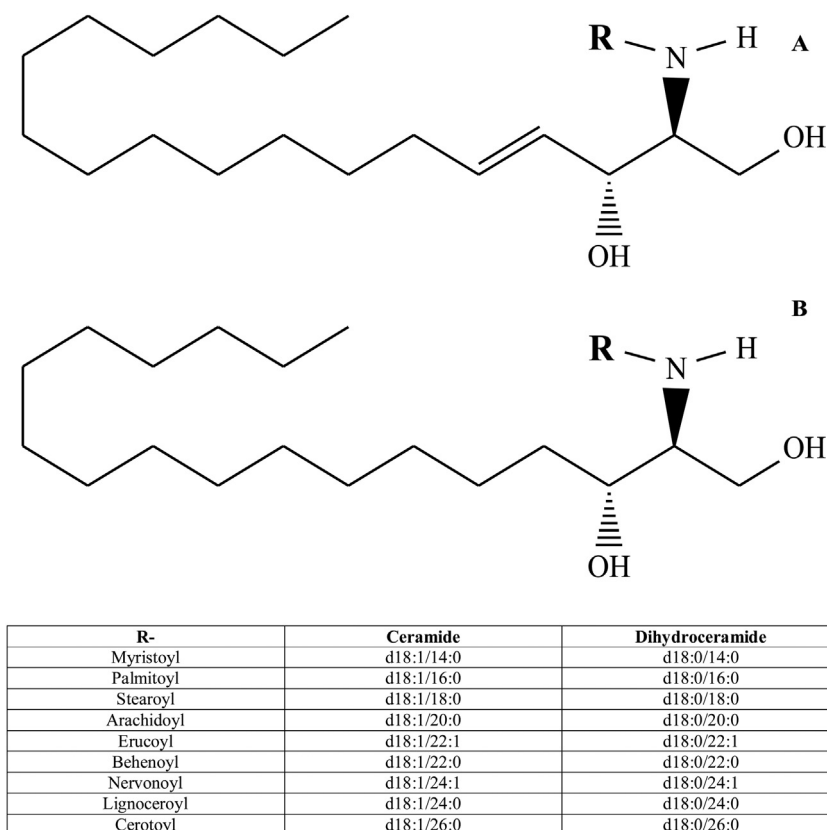| R-	Ceramide	Dihydroceramide
Myristoyl	d18:1/14:0	d18:0/14:0
Palmitoyl	d18:1/16:0	d18:0/16:0
Stearoyl	d18:1/18:0	d18:0/18:0
Arachidoyl	d18:1/20:0	d18:0/20:0
Erucoyl	d18:1/22:1	d18:0/22:1
Behenoyl	d18:1/22:0	d18:0/22:0
Nervonoyl	d18:1/24:1	d18:0/24:1
Lignoceroyl	d18:1/24:0	d18:0/24:0
Cerotoyl	d18:1/26:0	d18:0/26:0

Fig. 1. General structures and nomenclatures of ceramide (A) and dihydroceramide (B).

cell membranes, ceramides have also been recognized as bioactive signaling modulators for various essential cellular events, particularly cell proliferation, differentiation, migration, adhesion, and apoptosis [4].

In view of their potential proapoptotic toxicity in normal eukaryotic cells, ceramide levels are dynamically regulated by metabolic influx through the catabolism of sphingomyelins and metabolic outflux through the degradation of ceramides into sphingosine-1-phosphate, a bioactive sphingolipid that is known to promote cell survival by counteracting the apoptotic effect induced by elevated ceramides. This balancing effect of ceramide metabolism creates an interactive rheostat for subcellular machinery to exert its regular physiological functions [5].

In contrast, alternation of this rheostat between cell apoptosis and survival has been reported to contribute to abnormal early development of the placenta, characterized by compromised proliferation, differentiation, and apoptosis of trophoblast cells. Such changes could lead to persistent placental hypoxia and oxidative stress due to insufficient uteroplacental circulation from the maternal spiral arteries and eventually to the pathogenesis of a wide variety of major adverse pregnancy outcomes, including preeclampsia [6], ectopic pregnancy [7], intrauterine growth restriction [8], and recurrent miscarriage [9]. Dihydroceramides, although their associations with pregnancy have not been well characterized, recent evidence has suggested that they exert distinct biological functions that are complementary to the prevalent ceramides in a variety of related disorders, including autophagy and hypoxia [10,11]. Moreover, sphingolipids have been identified by a number of cross-gestational studies to be associated with early-onset preeclampsia in pregnancy women during the first trimester, underlying their pathological importance as candidate markers for early prediction of preeclampsia and other pregnancy-related disorders [12,13]. Therefore, in order to provide further insights into

various conditions of pregnancy, we undertook a population-based study to establish the physiological baseline levels of ceramides and dihydroceramides, including both odd- and even-chain species, during normal pregnancies.

To date, various analytical methodologies have been established for the measurement of ceramides in clinical specimens, such as immunochemistry [14]. However, these methods, in general, are limited by their narrow dynamic range, poor detection sensitivity, low analytic throughput, and inability to resolve individual ceramides at the molecular level, which precludes the expansion of their application to routine clinical analysis. Recently, the advent of high-performance liquid chromatography interfaced to tandem mass spectrometer (LC/MS/MS) has given rise to the development of ceramide assays with greater sensitivity, specificity, and throughput from complex biological matrices. Previously, Jiang et al. established a LC/MS/MS method for simultaneous quantification of ceramides (d18:1/22:0) and (d18:1/24:0) in human plasma [15], and Kauhanen et al. developed a high-throughput LC/MS/MS approach for routine clinical measurement of ceramides (d18:1/16:0), (d18:1/18:0), (d18:1/24:1), and (d18:1/24:0) in human plasma [16]. Both methods demonstrated good accuracy, precision, and throughput over clinically relevant ranges, but lack sufficient molecular coverage for the assay. Therefore, the expansion of the analytical capacity to include more ceramides and dihydroceramides in the assay would be useful.

In this study, we developed and validated a high-throughput LC/MS/MS method for parallel quantification of 16 ceramides and 10 dihydroceramides in human serum within 5 min by using stable isotope-labeled ceramides as internal standards (ISs). This method employs a protein precipitation method for quick sample preparation, reverse-phase isocratic elusion for chromatographic separation, and Multiple Reaction Monitoring (MRM) for mass spectrometric detection. The assay was validated against US FDA

guidelines for the lower limit of quantitation (LLOQ), linearity, precision, accuracy, extraction recovery, stability, and carryover. The validated assay was then applied to determine serological baselines of ceramides and dihydroceramides in cross-gestational normal pregnancies.

2. Materials and methods

2.1. Materials

All calibration standards including ceramides (d18:1/14:0), (d18:1/16:0), (d18:1/17:0), (d18:1/18:1), (d18:1/18:0), (d18:1/20:0), (d18:1/22:0), (d18:1/24:1), (d18:1/24:0), and dihydroceramides (d18:0/16:0), (d18:0/18:1), (d18:0/18:0), (d18:0/24:1) were purchased from Avanti Lipids (Alabaster, AL). Stable isotope-labeled ISs including d_7-ceramides (d18:1/16:0), (d18:1/18:0), (d18:1/24:1), and (d18:1/24:0) were also purchased from Avanti Lipids. HPLC grade water, MeOH, 2-propanol, and $CHCl_3$ were obtained from Fisher Scientific (Pittsburgh, PA). Analytical grade ammonium bicarbonate was purchased from Sigma Aldrich (St. Louis, MO). The de-lipidized serum VD-DDC Mass Spec Gold was obtained from Golden West Biological (Temecula, CA). All materials were directly used without further purification.

2.2. Human serum sample

Serum samples from 10 healthy human donors were purchased from the Stanford Blood Center (Palo Alto, CA). These samples were combined to generate a pooled serum sample for quality control (QC) purposes.

Clinical samples containing 29 maternal serum samples from full-term pregnancies without complication were purchased from ProMedDX Inc. (Norton, MA, USA, http://www.promeddx.com) and included detailed case report forms.

The study was approved by institutional review boards (IRB#:5136) at Stanford University and ProMedDX Inc. and conducted according to 21 CFR and ICH/GCP guidelines and HIPAA Privacy Regulations. Informed consent was obtained from every subject unless this requirement had been waived by the respective IRBs.

All serum samples were aliquoted and stored at −80 °C prior to analysis.

2.3. Stock and working solutions

Stock solutions of ceramides (d18:1/14:0), (d18:1/16:0), (d18:1/17:0), (d18:1/18:1), (d18:1/18:0), (d18:1/20:0), (d18:1/22:0), (d18:1/24:1), (d18:1/24:0) and dihydroceramides (d18:0/16:0), (d18:0/18:1), (d18:0/18:0), (d18:0/24:1) were prepared by dissolving the lyophilized powders in MeOH:$CHCl_3$ (1:1) to obtain a concentration of 5.00 mM.

A set of six-level calibrator working solutions were prepared by mixing and serially diluting stock solutions with 2-propanol to obtain concentrations at 1.00, 2.00, 10.0, 50.0, 2.00×10^2, 1.00×10^3 nM for ceramides (d18:1/14:0), (d18:1/17:0), (d18:1/18:1), (d18:1/18:0), (d18:1/20:0) and dihydroceramides (d18:0/16:0), (d18:0/18:1), (d18:0/18:0), (d18:0/24:1), and at 5.00, 10.0, 50.0, 2.50×10^2, 1.00×10^3, 5.00×10^3 nM for ceramides (d18:1/16:0), (d18:1/22:0), (d18:1/24:1), (d18:1/24:0).

A set of four-level QC working solutions were prepared by mixing and serially diluting stock solutions with 2-propanol to obtain concentrations at 1.00, 2.50, 1.00×10^2, 7.50×10^2 nM for ceramides (d18:1/14:0), (d18:1/17:0), (d18:1/18:1), (d18:1/18:0), (d18:1/20:0) and dihydroceramides (d18:0/16:0), (d18:0/18:1), (d18:0/18:0), (d18:0/24:1), and at 5.00, 12.5, 1.00×10^2, 3.75 $\times 10^3$ for ceramides (d18:1/16:0), (d18:1/22:0), (d18:1/24:1), (d18:1/24:0).

The stock solutions of d_7-ceramide (d18:1/16:0), (d18:1/18:0), (d18:1/24:1), and (d18:1/24:0) were prepared by dissolving the lyophilized powders in MeOH:$CHCl_3$ (1:1) to obtain a universal concentration at 1.00 mM. The IS working solution was prepared by mixing and serially diluting stock solutions with methanol to obtain concentrations at 5.00 nM for all stable isotope-labeled ceramides.

All prepared solutions and samples were stored at −20 °C prior to use.

2.4. Sample preparation

For the preparation of blank samples, a 10-μL aliquot of de-lipidized serum was spiked with 10 μL of 2-propanol. The blank samples were extracted with 200 μL of methanol and the IS working solution to obtain double and single blanks, respectively.

For the preparation of calibrators, a 10-μL aliquot of de-lipidized serum was spiked with 10 μL of calibrator working solution at the corresponding level. The spiked calibrators were individually extracted with 200 μL of the IS working solution to obtain a set of calibrators based on 6 concentration levels.

For the preparation of QC samples, a 10-μL aliquot of de-lipidized serum was spiked with 10 μL of the QC working solution at the corresponding level. The spiked QC samples were individually extracted with 200 μL of the IS working solution to obtain a set of 4 concentration levels.

For the preparation of serum samples, a 10-μL aliquot of the unknown sample was spiked with 10 μL of 2-propanol and extracted with 200 μL of the IS working solution.

Following the extraction, all extracted samples were subjected to vigorous vortex for 30 s and high-speed centrifuge at 12,000×g under 4 °C for 5 min. Thereafter, 180 μL of supernatant was removed from each sample and transferred into an auto-sampler vial with micro-insert for LC/MS/MS analysis.

2.5. LC/MS instrumentation

The Dionex Ultimate 3000 UHPLC system consisted of a degasser, a RS binary pump, a RS auto-sampler, and a RS column compartment from Thermo Fisher (San Jose, CA). The UHPLC system was interfaced with a TSQ Quantiva mass spectrometer equipped with electrospray ionization source and a built-in Rheodyne switch valve from Thermo Fisher. Data acquisition and chromatographic peak integration were implemented using the XCalibur 4.0 software package from Thermo Fisher.

2.6. LC///MS/MS procedure

Following sample preparation, 10 μL of the sample was injected onto an ACE Excel SuperC18 column (1.7 μm, 100 mm × 2.1 mm; MAC-MOD Analytical, Chadds, PA). 1 M of ammonium bicarbonate was diluted 100-fold by a mixture of methanol and 2-propanol (1:1) to obtain the mobile phase containing 10 mM of ammonium bicarbonate at pH around 7.2. Chromatographic separation was carried out using a 5-min isocratic elusion program. Briefly, the LC eluent was directed to the waste for the first 1.0 min and then switched back to the electrospray interface from 1.1 to 5 min, allowing the targeted ceramides and dihydroceramides to be sequentially eluted, ionized, and detected by the system. The flow rate was set constantly at 0.3 mL/min, and temperatures of the auto-sampler and column oven were maintained at 4 and 30 °C, respectively, throughout the analysis.

The mass spectrometer was operated in a scheduled MRM mode to continuously acquire data from the LC eluent. The retention time-dependent data acquisition was employed using pre-defined

Table 1
The optimized transitions for absolutely quantitated analytes.

Compound	Product Ion	RT (min)	RT Window (min)	Polarity	Precursor (m/z)	Product (m/z)	Collision Energy (V)	RF Lens (V)
Ceramide (d18:1/14:0)	Quantitative	1.58	1.20	Negative	508.5	252.3	27.19	121.0
	Qualitative	1.58	1.20	Negative	508.5	226.2	25.78	121.0
Ceramide (d18:1/16:0)	Quantitative	1.79	1.20	Negative	536.6	280.4	30.23	121.0
	Qualitative	1.79	1.20	Negative	536.6	254.3	26.94	121.0
Dihydroceramide (d18:0/16:0)	Quantitative	1.89	1.20	Negative	538.6	280.4	30.38	136.0
	Qualitative	1.89	1.20	Negative	538.6	237.3	35.08	136.0
Ceramide (d18:1/17:0)	Qualitative	1.91	1.20	Negative	550.6	294.4	28.96	101.0
	Quantitative	1.91	1.20	Negative	550.6	268.3	27.60	101.0
Ceramide (d18:1/18:1)	Qualitative	1.82	1.20	Negative	562.6	306.4	29.62	115.0
	Quantitative	1.82	1.20	Negative	562.6	280.3	26.53	115.0
Dihydroceramide (d18:0/18:1)	Qualitative	2.04	1.20	Negative	564.6	306.4	30.88	123.0
	Quantitative	2.04	1.20	Negative	564.6	263.3	30.58	123.0
Ceramide (d18:1/18:0)	Qualitative	2.04	1.20	Negative	564.6	308.4	31.29	129.0
	Quantitative	2.04	1.20	Negative	564.6	282.3	28.56	129.0
Dihydroceramide (d18:0/18:0)	Quantitative	2.18	1.20	Negative	566.6	308.4	31.44	140.0
	Qualitative	2.18	1.20	Negative	566.6	265.3	35.94	140.0
Ceramide (d18:1/20:0)	Quantitative	2.36	1.20	Negative	592.6	336.4	32.40	136.0
	Qualitative	2.36	1.20	Negative	592.6	310.3	29.97	136.0
Ceramide (d18:1/22:0)	Quantitative	2.74	1.20	Negative	620.7	364.5	34.52	132.0
	Qualitative	2.74	1.20	Negative	620.7	338.4	32.05	132.0
Ceramide (d18:1/24:1)	Quantitative	2.75	1.50	Negative	646.7	390.5	36.19	142.0
	Qualitative	2.75	1.50	Negative	646.7	364.4	30.83	142.0
Dihydroceramide (d18:0/24:1)	Quantitative	3.25	1.50	Negative	648.7	390.5	35.33	138.0
	Qualitative	3.25	1.50	Negative	648.7	347.4	35.33	138.0
Ceramide (d18:1/24:0)	Quantitative	3.25	1.50	Negative	648.7	392.5	34.62	145.0
	Qualitative	3.25	1.50	Negative	648.7	366.4	31.99	145.0

Table 2
The optimized transitions for approximately quantitated analytes and internal standards.

Compound	Product Ion	RT (min)	RT Window (min)	Polarity	Precursor (m/z)	Product (m/z)	Collision Energy (V)	RF Lens (V)
Ceramide (d18:1/20:1)	Quantitative	2.06	1.20	Negative	590.6	334.4	32.40	136.0
	Qualitative	2.06	1.20	Negative	590.6	308.3	29.97	136.0
Dihydroceramide (d18:0/20:0)	Quantitative	2.52	1.20	Negative	594.6	336.4	31.44	140.0
	Qualitative	2.52	1.20	Negative	594.6	293.3	35.94	140.0
Ceramide (d18:1/21:0)	Quantitative	2.54	1.20	Negative	606.6	350.4	32.40	136.0
	Qualitative	2.54	1.20	Negative	606.6	324.3	29.97	136.0
Dihydroceramide (d18:0/21:0)	Quantitative	2.72	1.20	Negative	608.6	350.4	31.44	140.0
	Qualitative	2.72	1.20	Negative	608.6	307.3	35.94	140.0
Ceramide (d18:1/22:1)	Quantitative	2.38	1.20	Negative	618.7	362.5	34.52	132.0
	Qualitative	2.38	1.20	Negative	618.7	336.4	32.05	132.0
Dihydroceramide (d18:0/22:0)	Quantitative	2.94	1.20	Negative	622.7	364.5	35.38	133.0
	Qualitative	2.94	1.20	Negative	622.7	321.4	35.33	133.0
Ceramide (d18:1/23:0)	Quantitative	2.99	1.50	Negative	634.7	378.5	34.52	132.0
	Qualitative	2.99	1.50	Negative	634.7	352.4	32.05	132.0
Dihydroceramide (d18:0/23:0)	Quantitative	3.22	1.50	Negative	636.7	378.5	35.38	133.0
	Qualitative	3.22	1.50	Negative	636.7	335.4	35.33	133.0
Ceramide (d18:1/24:2)	Quantitative	2.43	1.50	Negative	644.7	388.5	36.19	142.0
	Qualitative	2.43	1.50	Negative	644.7	362.4	30.83	142.0
Ceramide (d18:1/25:0)	Quantitative	3.50	1.50	Negative	662.7	406.5	34.62	145.0
	Qualitative	3.50	1.50	Negative	662.7	380.4	31.99	145.0
Dihydroceramide (d18:0/25:0)	Quantitative	3.80	1.50	Negative	664.7	406.5	35.33	138.0
	Qualitative	3.80	1.50	Negative	664.7	363.4	35.33	138.0
Ceramide (d18:1/26:0)	Quantitative	3.85	1.50	Negative	676.7	420.5	34.62	145.0
	Qualitative	3.85	1.50	Negative	676.7	394.4	31.99	145.0
Dihydroceramide (d18:0/26:0)	Quantitative	4.15	1.50	Negative	678.7	420.5	35.33	138.0
	Qualitative	4.15	1.50	Negative	678.7	377.4	35.33	138.0
d_7-Ceramide (d18:1/16:0)	Quantitative	1.79	1.20	Negative	543.6	280.4	30.23	121.0
d_7-Ceramide (d18:1/18:0)	Quantitative	2.04	1.20	Negative	571.6	308.4	31.29	129.0
d_7-Ceramide (d18:1/24:1)	Quantitative	2.72	1.50	Negative	653.7	390.5	36.19	142.0
d_7-Ceramide (d18:1/24:0)	Quantitative	3.22	1.50	Negative	655.7	392.5	34.62	145.0

retention time windows with variable widths (1.2 min. for medium chain and 1.5 min. for long chain ceramides and dihydroceramides) to record the extracted ion chromatograms (EIC) of targeted analytes. The MRM transitions for targeted ceramides and dihydroceramides were individually optimized by direct syringe pump infusion of 0.5 μM of the corresponding standards at 10 μL/min into the mass spectrometer in the presence of 10 mM of ammonium bicarbonate. The optimized MRM transitions with scheduled retention times are given in Tables 1 and 2 for absolutely quantitated analytes, approximately quantitated analytes, and stable isotope-labeled internal standards. The Q1 and Q3 resolutions were both set at 0.7 Da, and the cycle time was set at 1 s.

In addition, the source parameters were also optimized by in-source mixing of the mobile phase flow at 0.3 mL/min with continuous infusion of 0.5 μM of standard cocktail at 10 μL/min via a tee connector. The spray voltage was optimized at −3500 V, and the optimal gas flows were determined to be 30, 10, and 0 Arb for Sheath Gas, Aux Gas, and Sweep Gas, respectively. The temperatures for ion transfer tube and vaporizer were also optimized to be both at 300 °C.

2.7. Qualification

The qualification of targeted ceramides and dihydroceramides was implemented via a two-step process according to the response ratio of pairwise product ions as recommended by CLSI guideline [17].

In the first step, the chromatographic peak areas of both quantitative and qualitative ions were integrated for absolutely quantitated analytes from Table 1 based on their retention times in corresponding EICs across all calibrators, QCs, and serum samples. The integrated peak areas were first manually inspected, normalized by their labeled counterparts/analogs, and then calculated for product ion ratios by dividing the area under curve (AUC) of quantitative ions by the AUC of qualitative ions. In order for the absolutely quantitated analytes to be accepted for the subsequent quantitation process, they must be qualified to show the product ion ratios of serum samples have less than 10 % deviations in relative to the mean product ion ratio of calibrator and QC samples.

In the second step, the chromatographic peak areas of both quantitative and qualitative ions were integrated for approximately quantitated analytes from Table 2 based on their observed retention times in corresponding EICs across all serum samples. The integrated peak areas were first manually inspected, normalized by their labeled counterparts/analogs, and then calculated for product ion ratios by dividing the AUC of quantitative ions by the AUC of qualitative ions. In consideration of the unavailability of commercial standards for the approximately quantitated analytes, a 20 % acceptance cutoff was set on the product ion ratios of serum samples in relative to the mean product ion ratio of calibrator and QC samples from their assigned analogs for qualification based on a pre-defined relationship.

The relationships for normalization and qualification are detailed in Supplemental Table 1.

2.8. Quantitation

The quantitation of targeted ceramides and dihydroceramides was implemented via two separate approaches.

In the first approach, known as absolute quantitation, the IS-normalized peak area ratios for absolutely quantitated analytes from Table 1 were plotted against the spiked concentrations in calibrators to establish calibration curves based on 6 levels. Linear regression fitting with a weighting factor of $1/x^2$ was employed for the calibration. Thereafter, a >0.99 cutoff was set on the square of the correlation coefficient to ensure that individual calibration curves were qualified for quantitation. After that, the IS-normalized peak area ratios of targeted analytes were plugged into the corresponding calibration curves to obtain absolutely quantitated concentrations in blank, QC, and serum samples.

In the second approach, known as approximate quantitation, the IS-normalized peak area ratios for approximately quantitated analytes from Table 2 were plugged into the assigned calibration curves based on a pre-defined relationship to obtain approximately quantitated concentrations in the serum samples.

The relationship for quantitation is detailed in Supplemental Table 1.

2.9. Statistic analysis

For the clinical application, spearman test was used to determine the correlation coefficient between analyte concentrations and gestational age (GA). The quadratic polynomial fitting was used to visualize the gestation-concentration correlations. Due to the limited sample size, Kruskal-Wallis H-test, a non-parametric version of ANOVA, was used to compare levels of each ceramides/dihydroceramides among three gestational age groups and determine the statistical significance. Locally estimated scatterplot smoothing (LOESS) based on local quadratic polynomial regression analysis was utilized to establish the gestational baseline for normal pregnancy based on significant analytes.

3. Result and discussion

3.1. MS condition

Electrospray ionization interfaced with tandem mass spectrometer (ESI-MS/MS) appears to be a more advantageous platform than the immuno-based approach for analysis of ceramides, considering its superior selectivity to unambiguously differentiate molecular ceramides with major structural resemblance, which would be technically challenging for the immune-based method due to the significant inter-ceramide cross-reactivity observed with the antibodies [14]. The ionization mechanisms and in-depth structural characterization of collision-induced dissociation (CID) fragments have been well documented for ceramides in ESI-MS/MS [18,19]. In ESI + mode, the ionization of ceramides generally takes place at the carbonyl oxygen from the C2 amide linkage via the addition of a single proton, which, upon dissociation, generates a characteristic fragment at 264.3 *m/z*, corresponding to the protonated d18:1 sphingosine ion after the loss of two water molecules. This signature fragment represents the essential d18:1 sphingosine building block, which forms the principal infrastructure for both qualitative and quantitative analysis of ceramides by ESI + . However, due to the fragile nature of hydroxy groups, significant in-source dehydration from protonated molecular ions has been observed on the ceramides during the ionization in ESI+, leading to reduced abundance of molecular ions and thus diminished detection sensitivity [18]. In ESI- mode, the ceramide undergoes ionization by removing a proton from the C2 amide nitrogen and, upon dissociation, produces a wide spectrum of structurally informative fragments, featured by the neutral loss (NL) of 256.2 *m/z*, corresponding to the loss of a hexadecenal and water molecules. The fragment generated by NL of 256.2 *m/z* in ESI- has been demonstrated to be a superior fragment over the 264.3 *m/z* fragment in ESI + for both qualitative and quantitative analysis, as it is not limited by the detrimental in-source dehydration phenomenon observed during the protonation. However, the deprotonation of ceramides in ESI- could be severely affected by the presence of chloride ion, a direct competitor for the uncharged ceramide molecule during ionization, significantly dropping the abundance of the deprotonated molecular ion by forming the chloride adduct [19]. In this study, ESI- was selected as the method for ionization over ESI + based on the following rationales: 1) once dissociated, the molecular ion of ceramide in ESI- produces more structurally informative fragments than ESI+, allowing the unambiguous identification and quantification of ceramides in extremely complex biological matrices; 2) the signal-diluting effect imposed by the chloride ion on ionization in ESI- could be practically overcome by separating the sample across a hydrophobic stationary phase to deplete the chloride ion and enrich the molecular ceramides prior to ionization; 3) elimination of the in-source dehydration phenomenon in the negative ionization efficiently preserves the deprotonated molecular ion of ceramide to the maximal extent, therefore boosting detection sensitivity.

The representative product ion spectra are shown in Fig. 2 for ceramide (d18:1/18:0) and dihydroceramide (d18:0/18:0). As illustrated by their MS/MS fingerprints, ceramide (d18:1/18:0) could be readily identified by the presence of N-vinyloctadecanamide and octadecanamide anions generated by the NL of 256.2 and 282.3 *m/z* from the molecular ion, whereas dihydroceramide (d18:0/18:0), which differs by one less double bond, was characterized by the
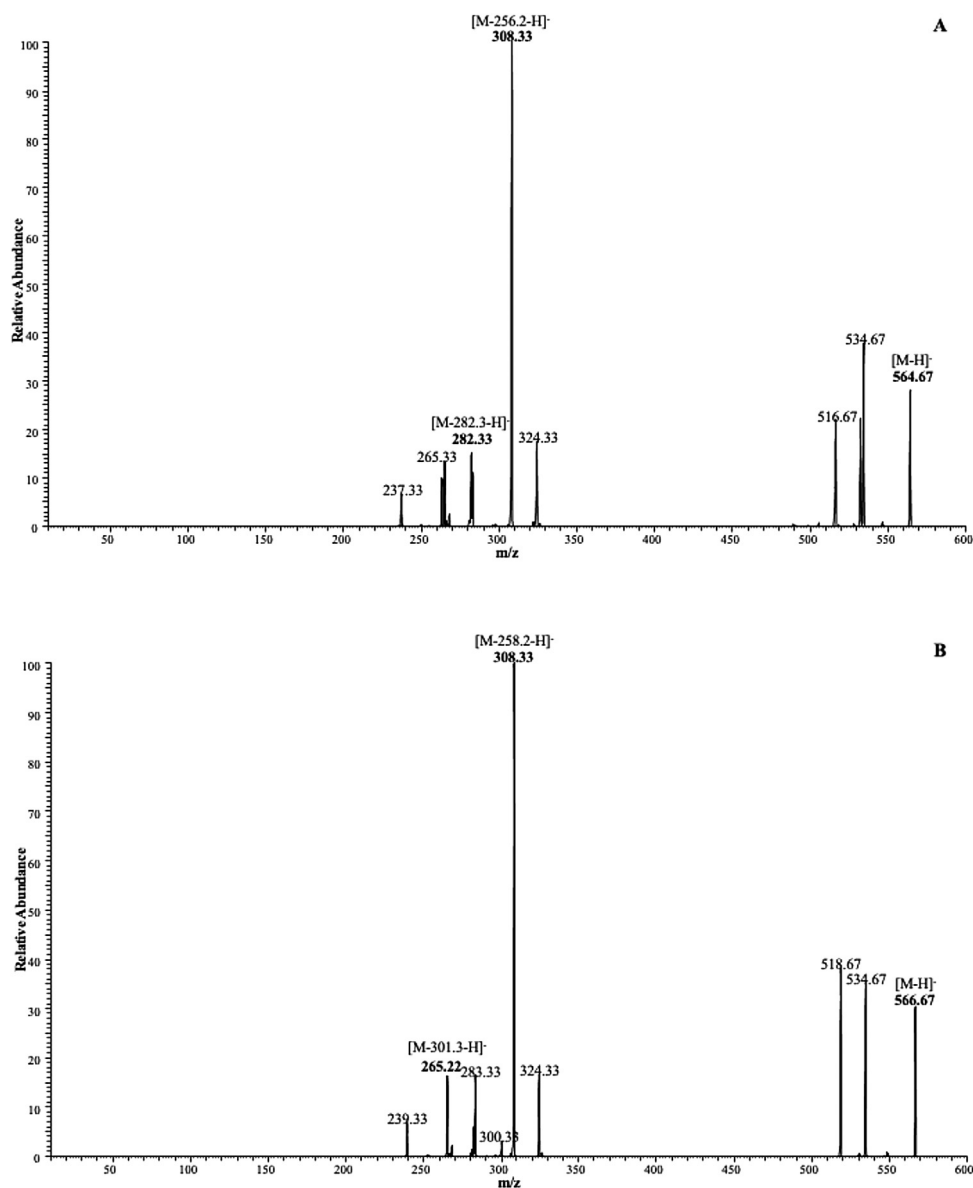
Fig. 2. Fragmentation spectra of ceramide (d18:1/18:0) (A) and dihydroceramide (d18:0/18:0) (B).

presence of N-vinyloctadecenamide and hexadecylketene anions produced by the NL of 258.2 and 301.3 m/z from the molecular ion. In addition, the fragments created by the NL of 256.2 and 258.2 m/z were found to be the most abundant product ions for ceramides and dihydroceramides, respectively. These observations were consistent with the previous finding [19].

To assure the sensitivity and specificity of the MS detection, multiple fragments were selected as product ion candidates and paired with [M−H]$^-$ as the precursor ion to be evaluated in terms of absolute abundance, fragmentation reproducibility, and robustness to interference for the targeted analysis by MRM. Following the evaluation, the product ions [M−H−256.2]$^-$ and [M−H−282.3]$^-$ from ceramides were observed to outweigh others for quantitative and qualitative analysis, respectively. Likewise, the product ions [M−H−258.2]$^-$ and [M−H−301.3]$^-$ from dihydroceramides were identified to be superior over others for quantitative and qualitative analysis, respectively. The optimized SRM transitions are listed in Tables 1 and 2. The fragmentation mechanisms of 256.2 and 282.3 m/z NL for ceramides and 258.2 and 301.3 m/z NL for dihydroceramides are shown in Fig. 3.

3.2. LC condition

According to previous studies [20,21], a prior chromatographic separation step is essential to alleviate the charging competition that occurs between co-eluting analytes and matrix components and minimize the extent of ionization suppression introduced onto the targeted analytes, thus improving the sensitivity, specificity, and robustness of the assay. Among multiple chromatographic platforms, reverse phase chromatography is known for its capability to retain and separate lipophilic molecules in an order of increasing hydrophobicity, and its application is fundamental for the chromatographic separation of hydrophobic molecules to take place in a highly reproducible manner. In view of the hydrophobic nature of ceramides and dihydroceramides as complex sphingolipids, an ACE Excel SuperC18 UPLC column (1.7 μm, 100 mm × 2.1 mm) was therefore selected for chromatographic separation to provide reliable matrix cleanup and analyte enrichment prior to the ionization.

Moreover, in the existing methodologies, gradient elusion programs were preferentially employed for the analysis of ceramides to improve chromatographic resolution and detection sensitivity.
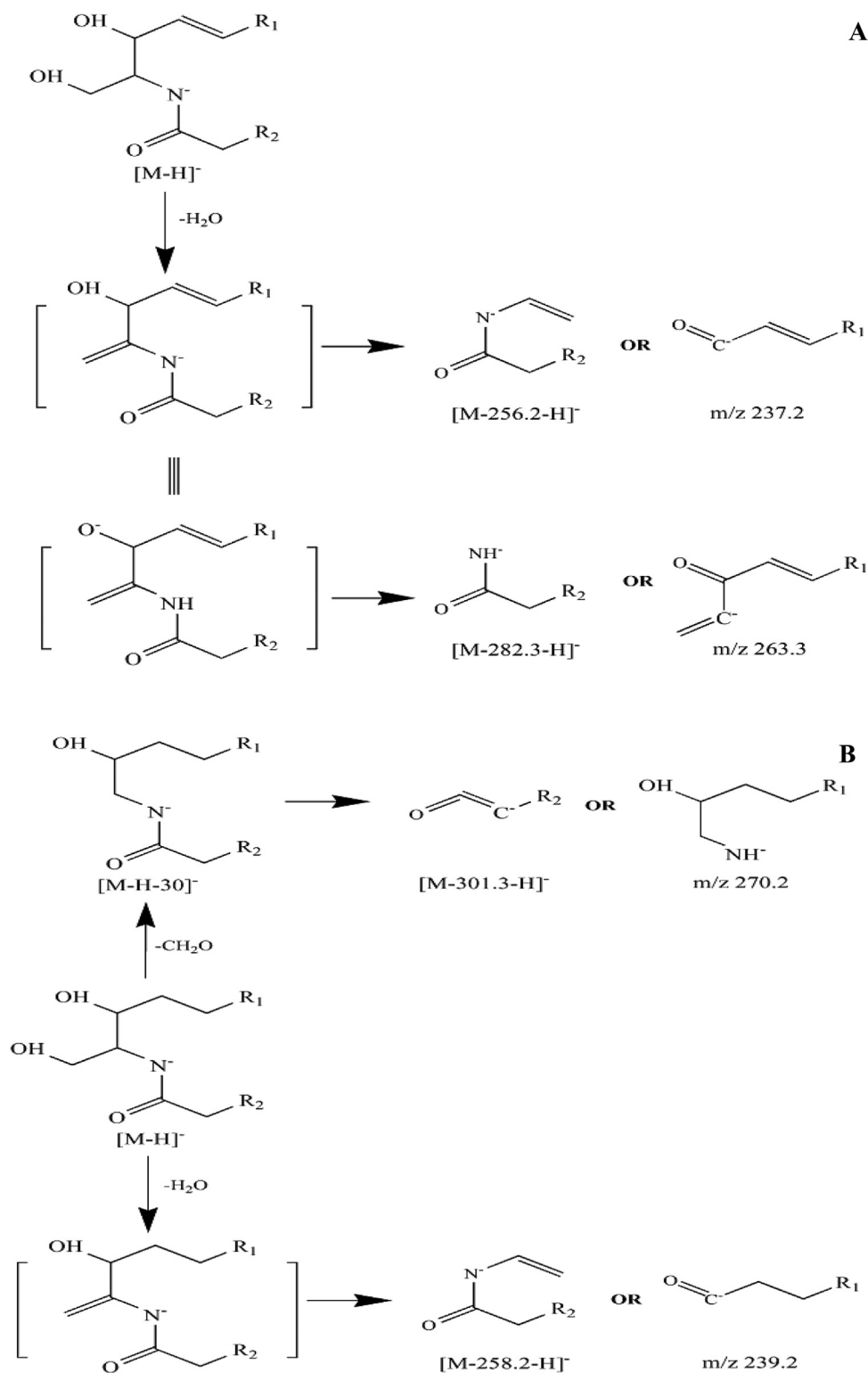
Fig. 3. Fragmentation mechanism of NL 256.2 and 282.3 *m/z* for ceramide (A) and NL 258.2 and 301.3 *m/z* for dihydroceramide (B).

Based on published data, utilization of gradient elusion programs allows the targeted ceramides to be retained, separated, and eluted reproducibly with excellent run-to-run consistency [20,21]. However, as the tradeoff of improved chromatographic resolution and detection sensitivity, gradient elusion is also technically subjected to a number of limitations. On one hand, the continuously variable mobile phase percentage program used by gradient elusion unfavorably influences the stability of the chromatographic base-line, causing the baseline to fluctuate constantly throughout the analysis. On the other hand, gradient elusion inevitably requires additional chromatographic periods for column cleanup and re-equilibration, leading to a shortened analyte elusion window, prolonged running time, and extended instrument idle period. As an alternative, isocratic elusion seems to be a potential solution to circumvent these shortcomings. In practice, isocratic elusion renders a more stabilized chromatographic baseline with minimal
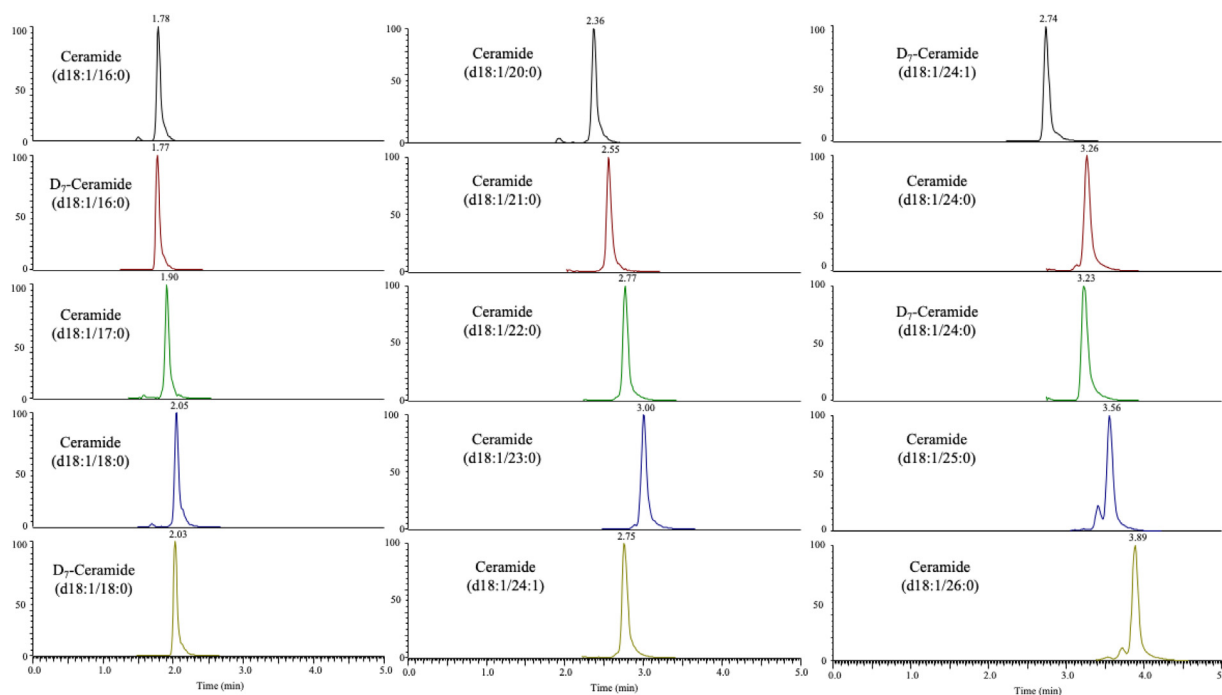
Fig. 4. The representative EICs of different ceramides in real serum extract under the isocratic elusion. The X-axis is retention time, and Y-axis is relative intensity.

column cleanup and re-equilibration steps required. Unfortunately, isocratic elusion also suffers from pitfalls such as a broadened chromatographic peak, prone to column overloading, and enhanced sample carryover. Therefore, in the course of method development, a number of vital chromatographic parameters including mobile phase composition, sample loading solvent, column oven temperature, flow rate, sample injection volume, and running time were individually and collectively optimized to obtain improved chromatographic resolution with sharpened peaks in the absence of column overloading. The sample carryover was also evaluated under optimized conditions to be negligible from sample to sample. It is worth noting that with the use of methanol, both as extraction solvent and sample loading solvent, the width of the chromatographic peak was significantly narrowed to achieve for increased signal intensity and a lowered detection limit. In addition, the inclusion of 2-propanol in the mobile phase minimizes the buildup of hydrophobic matrix components onto the column over time and improves the elution of targeted analytes with sharpened chromatographic peaks and a shortened analytical run. Under our optimized conditions, the targeted ceramides and dihydroceramides were consistently eluted off the column from 1.5 to 4.5 min in an order of increased hydrophobicity with negligible shift on retention times over hundreds of sample injections. The representative EICs of different ceramides are given in Fig. 4 to demonstrate the separation performance. As shown by Fig. 4, The chromatographic peak widths of our analytes were between 15 and 20 s, and a cycle time of 1 s could therefore generate 15~20 data points for a single peak, which is sufficient for quantitation. In addition, the scheduled selected reaction monitoring based on the distinct retention time windows of our analytes was utilized to provide a good balance between the signal count and the duty cycle.

Chemically, the pKa value for the amide N—H bond on ceramide should range from 25 to 26, suggesting that the amide nitrogen is essentially a weak acid and very unlikely to donate its proton under acidic or neutral pH. However, in the presence of a base in large excess, the acid-base interaction would be expected to facilitate the proton-donating process on the amide N—H bond, stabilize the amide nitrogen anion that is generated, and thus increase ion-

ization efficiency. Furthermore, in consideration of the subsequent detection phase, the base being used must be a volatile chemical that is compatible with the ESI interface and MS analysis, ranking the ammonium bicarbonate buffer the top candidate on the list. Moreover, as the majority of C18 reverse phase columns are unable to be operated under basic pH owing to the chemical hydrolysis that might occur between the alkyl stationary phase and the silica bed, the ACE Excel SuperC18 UPLC column we selected for the analysis was further confirmed by the manufacturer to possess a stable alkyl stationary phase under extended pH range from 2 to 11, allowing the high pH chromatographic separation to be carried out with promising robustness.

3.3. Extraction condition

Previous studies have demonstrated that the direct precipitation of serum/plasma proteins with the addition of organic solvents, such as methanol and 2-propanol, provides satisfactory extraction recovery (>80 %) for median- and long-chain ceramides across their physiological concentration ranges [15,16]. In addition, the depletion of endogenous proteins by organic solvents from serum/plasma samples, while coupled with online chromatographic separation and tandem mass spectrometric detection, has been shown to be a robust workflow to mitigate the potential interfering effects induced by the matrix, allowing sub-nM sensitivity to be achieved for the analysis of ceramides [15,16]. Finally, owing to the ease of handling, protein precipitation method has also been found to be highly automatable to accommodate for the large-scale analysis in a high-throughput fashion [15,16]. Therefore, protein precipitation was selected as the principal extraction strategy for our analysis.

Additionally, in view of the polarity of the mobile phase, 3 solvent combinations, including methanol, acetonitrile, and 2-proponol, were evaluated for their analyte-recovering and protein-precipitating capabilities from the pooled serum samples. Based on the results, we found that all 3 combinations provided equivalent degree of protein depletion from the sample at a sample-to-solvent ratio of 1:10 (v/v) or above, and repetitive injections of

serum samples extracted by all 3 combinations didn't increase the back pressure of the system. However, as compared to methanol and 2-propanol, we observed significantly reduced recoveries of ceramides and dihydroceramides from the pooled serum samples while using acetonitrile as the extraction solvent. Moreover, although comparable levels of analyte recovery by both methanol and 2-propanol extractions were observed, the chromatographic peak widths were substantially broadened with the injection of the 2-propanol extract in comparison with the methanol extract at the same volume, suggesting the increased polarity of the loading solvent dramatically decreases the analyte diffusion in the course of chromatography. Methanol was therefore selected as the solvent for both analyte extraction and sample loading.

Finally, two sample-to-solvent ratios, 1:10 and 1:20 (v/v), were also investigated to optimize the extraction methodology. From the comparative analysis, 1:10 ratio was found to provide higher S/N at the low concentration but was more prone to column overloading at the high concentration than 1:20 ratio, which leads to unfavorable peak broadening and retention time shifting and undermines the dynamic range of the quantitation. Hence, 1:20 was selected as the sample-to-solvent ratio for the final extraction protocol.

3.4. Approximate quantitation

Approximate quantitation, known as the approximate determination of certain molecules by referencing their signal responses to the calibration of resembled structural analogs established in the same matrix, has been used as an alternative method to circumvent the obstacles pertaining to conventional calibration using a one-to-one matched standard, and to provide approximately quantitative insights into molecules with unusual structures in the absence of commercial standards. The application of this approximate quantitation approach has been exemplified by the shotgun lipidomic analysis [22]. In those analysis, lipid standards with unnatural fatty acid moieties but identical lipid head groups to the analytes were selected as class-specific representatives to build the concentration-dependent calibration in the studied samples, which is then used as the known references to obtain quantitative information from the targeted analytes within the same lipid class by approximate quantitation. In view of the distinctive structural diversity of lipids, the utilization of exogenous analogs as class-specific representative calibrators has been demonstrated to analytically bypass the interfering signals originating from the endogenous lipids, simplifying the overall calibration process, and thus allowing the simultaneous quantitation of hundreds of lipid species from the sample in a rapid and reproducible fashion, paving the way for the shotgun lipidomic analysis. A number of prerequisites were proposed to be essential for the qualification of the approximate quantitation approach: 1) the molecular moiety that is subjected to structural variation should have minimal influence on the ionization efficiency, 2) the representative analogs selected for calibration should be structurally homologous to the targeted analytes, and 3) the linearity of representative calibrators should be demonstrated a priori in the matched matrix across the relevant concentration ranges. As mentioned above, for ceramides and dihydroceramides, the deprotonation process for negative ionization is predominantly undertaken at the nitrogen proton from the amide-linkage, and the variation on aliphatic chain length and saturation degree are expected to account for minimal impact on ionization efficiency. In addition, the linearities of representative ceramides and dihydroceramides with greatest structural similarities to the approximately quantitated analytes were established in the matched matrix over the meaningful concentration ranges, making the approximate quantitation approach as the most favorable strategy for measurement of those unusual ceramides and dihydroceramides in the clinical samples. Finally, since the complexity of the matrix components raises concerns about the validity of the detected signal from the human serum sample, especially on the approximately quantitated analytes, approximately quantitative results obtained from clinical samples were required to undergo a series of qualification procedures against the pre-defined acceptance criteria to ensure the selectivity of the measurement.

3.5. Method validation

The developed method was validated against the bioanalytical method validation guideline published by the US FDA in 2018 to evaluate for LLOQ, linearity, precision, accuracy, extraction recovery, stability, and carryover [23].

3.5.1. Surrogate matrix

Analytically, ceramides and dihydroceramides are endogenous molecules that presented at distinct abundances in human serum, and their serological concentrations could differ from each other up to a range of 3 orders of magnitude under different physiological conditions. However, the specific depletion of ceramides and dihydroceramides from the serum/plasma remains to be technically challenging. According to the 2018 bioanalytical guideline from US FDA for industry, the use of analyte-free matrix is recommended for quantitation of endogenous molecules in the biological matrix, and while obtaining the analyte-free matrix appears to be difficult, the use of surrogate matrix with systematic characterization is considered to be appropriate [23]. In the case of ceramide and dihydroceramide analysis, previous methodologies have adopted this surrogate matrix concept and explored the feasibility of performing the quantitation using 2-propanol and 5% bovine serum albumin solution as surrogate matrices, and both methodologies have demonstrated good robustness, sensitivity, and specificity in human plasma with proper validation steps [15,16]. In addition, previous study has also shown that de-lipidized serum serves as a good surrogate matrix for the analysis of endogenous steroid hormones in human serum and demonstrated that the established assay provides satisfactory performance according to guidelines from CLSI for routine clinical practice [24]. Based on these reported evidences, we therefore selected de-lipidized serum as the surrogate matrix for our assay to best mimic the matrix composition in the real serum sample. From our observations, our analytes behave similarly between de-lipidized and real serums in terms of retention time, fragmentation pattern, and signal-to-noise, allowing quantitation to be implemented in a highly confident fashion.

3.5.2. LLOQ

The LLOQ, defined as the concentration level with S/N > 10, for each absolutely quantitated analyte was determined by spiking the corresponding unlabeled standard at known concentration into the de-lipidized serum and then serially diluting the spiked serum sample with de-lipidized serum until S/N = 10 was reached in six replicates. In addition, the double blank and single blank samples were also analyzed in parallel to ensure that the baseline signal intensity from presented interference consistently accounted for <10 % of the signal intensity at the LLOQ for all targeted analytes. The determined LLOQ levels are given in Table 3.

3.5.3. Linearity

The linearity of the calibration curve, defined as the square of correlation coefficient (r^2) of the linear regression curve, was determined for each absolutely quantitated analyte based on 6 concentration levels with a weighting factor of $1/x^2$. The linear ranges were from 1.00 to 1.00×10^3 nM for ceramides (d18:1/14:0), (d18:1/17:0), (d18:1/18:1), (d18:1/18:0), (d18:1/22:0) and dihydroceramides (d18:0/16:0), (d18:0/18:1), (d18:0/18:0), (d18:0/24:1), and from 5.00 to 5.00×10^3 nM for

Table 3
The lower limit of quantitation, linear range, and linearity of individual calibration curves.

Analyte	LLOQ (nM)	Linear Range (nM)	Weighting Factor	R^2	Calibration Curve Equation
Ceramide (d18:1/14:0)	1.00	$1.00-1.00 \times 10^3$	$1/X^2$	0.999	Y = -0.00022648 + 0.0092549*X
Ceramide (d18:1/16:0)	5.00	$5.00-5.00 \times 10^3$	$1/X^2$	0.999	Y = 0.00904432 + 0.0116833*X
Ceramide (d18:1/17:0)	1.00	$1.00-1.00 \times 10^3$	$1/X^2$	0.999	Y = 0.00051912 + 0.0128024*X
Ceramide (d18:1/18:1)	1.00	$1.00-1.00 \times 10^3$	$1/X^2$	0.999	Y = 0.00003149 + 0.0148810*X
Ceramide (d18:1/18:0)	1.00	$1.00-1.00 \times 10^3$	$1/X^2$	0.999	Y = 0.00149927 + 0.0100025*X
Ceramide (d18:1/20:0)	1.00	$1.00-1.00 \times 10^3$	$1/X^2$	1.000	Y = 0.00057816 + 0.0107459*X
Ceramide (d18:1/22:0)	5.00	$5.00-5.00 \times 10^3$	$1/X^2$	0.999	Y = -0.00134115 + 0.0080520*X
Ceramide (d18:1/24:1)	5.00	$5.00-5.00 \times 10^3$	$1/X^2$	0.999	Y = 0.00489232 + 0.0087511*X
Ceramide (d18:1/24:0)	5.00	$5.00-5.00 \times 10^3$	$1/X^2$	0.999	Y = 0.01361550 + 0.0075987*X
Dihydroceramide (d18:0/16:0)	1.00	$1.00-1.00 \times 10^3$	$1/X^2$	1.000	Y = 0.00464943 + 0.0163816*X
Dihydroceramide (d18:0/18:1)	1.00	$1.00-1.00 \times 10^3$	$1/X^2$	0.999	Y = 0.00016294 + 0.0132201*X
Dihydroceramide (d18:0/18:0)	1.00	$1.00-1.00 \times 10^3$	$1/X^2$	0.999	Y = 0.00215833 + 0.0125412*X
Dihydroceramide (d18:0/24:1)	1.00	$1.00-1.00 \times 10^3$	$1/X^2$	0.999	Y = -0.00045146 + 0.0113406*X

ceramides (d18:1/16:0), (d18:1/20:0), (d18:1/24:1), (d18:1/24:0). The r^2 values for all calibration curves, which are presented in Table 3, were >0.99.

3.5.4. Precision and accuracy

The precision, defined as the coefficient of variation (CV%) of multiple measurements based on multiple sampling of the same homogenous sample, and accuracy, defined as the percent error (PE%) of the determined value relative to the nominal value, were evaluated for intra- and inter-assay measurements by analyzing QC samples prepared at four different concentrations, namely LLOQ, Low, Medium, and High, in six replicates for four independent runs. As shown in Supplemental Table 2, the CV% and PE% were below 11.9 and 10.6 % for the intra-assay measurement and below 6.57 and 9.53 % for inter-assay measurement. In addition, the QC pooled serum sample was prepared and analyzed in a similar setting to assess the precision of the approximately quantitated analytes for intra- and inter-assay measurements, considering the pure unlabeled standards were not commercially available for those analytes. As shown in Supplemental Table 3, the CV% values were below 8.85 and 13.3 % for intra- and inter-assay measurements, respectively, demonstrating the reproducibility of the assay.

3.5.5. Extraction recovery

Extraction recovery, defined as a percentage of the known amount of an analyte carried through the sample extraction and processing steps of the method, was evaluated for the extraction protocol by comparing two sets of QC samples prepared at three different concentrations, namely Low, Medium, and High, that undergo analyte spiking before and after the extraction in four replicates. As shown in Supplemental Table 4, the percentage recovery values were above 89.4 % for all analytes at studied concentrations, indicating insignificant loss of the analytes during sample extraction and processing steps.

3.5.6. Stability

Stability, defined as the percentage of intact analyte in a given matrix under specific storage and use conditions relative to the starting amount for a given interval, was evaluated for autosampler, benchtop, and long-term storage scenarios by analyzing four sets of QC samples prepared at three different concentrations, namely Low, Medium, and High, that undergo storage at specific conditions. The storage conditions were 24 h at 4 °C, 4 h at room temperature, and 21 days at −20 °C for auto-sampler, benchtop, and long-term stabilities, respectively. As shown in Supplemental Table 4, the stability percentages were above 83.2 % for all analytes under all conditions, suggesting minimal loss of analytes during storage.

Table 4
Demographic table.

Characteristic	Normal Pregnancy n = 29
Ethnicity	
African American	9 (31.0 %)
Hispanic	19 (65.5 %)
Other	1 (3.4 %)
Age (year)	
mean (SD)	25.4 (6.7)
Week of gestation[*]	
mean (SD)	33.6 (4.3)

[*] The time of blood drawing.

3.5.7. Matrix effect

Matrix effect, defined as a direct or indirect alteration or interference in response because of the presence of unintended analytes (for analysis) or other interfering substances in the sample, was evaluated by comparing two sets of QC samples in parallel at three different concentrations, namely Low, Median, and High, that were prepared in de-lipidized serum and methanol, respectively. As shown in Supplemental Table 4, the percent signal suppressions in the presence of matrix were determined to range from 19 to -40 % with standard deviation below 15 % across replicates for all analytes, which suggests the differential degrees of interactions between the individual analytes and the matrix components in the course of separation and detection, leading to consistent enhancement or suppression of the signal responses from the analytes.

3.5.8. Carryover

Carryover, defined as the appearance in a sample of an analyte from the proceeding sample, was evaluated by analyzing the calibrator sample with the highest analyte concentrations followed by the injection of a single blank sample with no analytes presented. The carryover effect was determined to be below 0.01 % for all analytes by including a needle washing step, both before and after the injection, with methanol. In addition, we also evaluated the carryover effect by injecting a double blank following the injection of a batch of 50 serum samples and observed no detectable signal responses from analytes in the double blank sample, suggesting the absence of carryover effect under our optimized conditions.

3.6. Method application

The ceramides and dihydroceramides in sera from 29 normal pregnancies were measured using the validated method. The cohort demographics are given in Table 4, and the determined concentrations are summarized in Table 5. The mean concentrations of ceramides (d18:1/16:0), (d18:1/18:0), and (d18:1/24:1) over all samples were 2.70×10^2, 0.99×10^2, and 7.69×10^2 nM, respectively, which were in line with the clinical reference

Table 5

Levels of ceramides and dihydroceramides from the application study.

| Analyte	24–29 Weeks (n = 7) Median Concentration (95 % CI) (nM)	30–33 Weeks (n = 5) Median Concentration (95 % CI) (nM)	34–40 Weeks (n = 17) Median Concentration (95 % CI) (nM)	Spearman Correlation Coefficient With GA	Kruskal-Wallis H-test p Value
Ceramide (d18:1/14:0)	10.4 (9.2–13.1)	5.5 (4.2–8.4)	8.0 (7.2–9.3)	−0.29	0.01
Ceramide (d18:1/16:0)	2.9×10^2 (2.4–4.3)$\times 10^2$	2.3×10^2 (2.0–2.5) $\times 10^2$	2.6×10^2 (2.3–2.8)$\times 10^2$	−0.16	0.06
Ceramide (d18:1/18:1)	5.4 (3.9–7.2)	3.9 (3.4–5.6)	5.5 (5.2–6.9)	0.34	0.18
Ceramide (d18:1/17:0)	4.4 (3.8–4.8)	3.4 (2.8–3.9)	3.9 (3.6–4.5)	0.08	0.09
Dihydroceramide (d18:0/16:0)	35.3 (29.5–58.7)	31.0 (28.4–34.2)	33.0 (30.5–45.9)	−0.01	0.52
Ceramide (d18:1/18:0)	99.9 (65.6–163.3)	61.0 (49.7–97.8)	1.0×10^2 (0.9–1.1) $\times 10^2$	0.22	0.20
Dihydroceramide (d18:0/18:1)	DQ	DQ	DQ	NA	NA
Dihydroceramide (d18:0/18:0)	28.8 (19.1–37.2)	19.5 (13.6–27.5)	24.5 (22.4–34.9)	0.18	0.51
Ceramide (d18:1/20:0)	82.9 (59.8–144.2)	56.4 (47.1–78.0)	93.7 (75.6–97.2)	0.19	0.12
Ceramide (d18:1/22:0)	5.9×10^2 (4.6–10.1)$\times 10^2$	5.4×10^2 (3.9–5.9)$\times 10^2$	5.5×10^2 (4.8–6.1)$\times 10^2$	−0.02	0.34
Ceramide (d18:1/24:1)	7.7×10^2 (5.8–12.5)$\times 10^2$	5.9×10^2 (4.7–6.4)$\times 10^2$	6.8×10^2 (6.2–9.2)$\times 10^2$	0.06	0.10
Dihydroceramide (d18:0/24:1)	68.2 (51.3–121.6)	69.5 (46.9–79.4)	84.1 (67.3–111.0)	0.12	0.69
Ceramide (d18:1/24:0)	2.0×10^3 (1.6–3.2)$\times 10^3$	1.7×10^3 (1.3–2.0)$\times 10^3$	1.6×10^3 (1.4–1.9)$\times 10^3$	−0.21	0.20
Ceramide (d18:1/20:1)	3.2 (2.4–4.2)	2.6 (2.2–3.4)	3.9 (3.4–4.8)	0.40	0.06
Ceramide (d18:1/22:1)	21.4 (16.4–27.6)	16.1 (14.5–19.4)	24.5 (21.1–30.9)	0.34	0.08
Ceramide (d18:1/24:2)	83.1 (71.0–122.3)	52.3 (45.8–68.5)	78.3 (70.7–110.8)	0.01	0.03
Ceramide (d18:1/21:0)	12.4 (10.5–17.7)	10.1 (7.35–13.0)	13.2 (11.6–15.2)	0.09	0.20
Dihydroceramide (d18:0/20:0)	15.6 (12.4–24.2)	13.1 (10.5–16.4)	15.1 (13.9–20.2)	0.10	0.57
Dihydroceramide (d18:0/21:0)	2.0 (1.8–2.2)	2.0 (1.4–2.4)	2.2 (1.7–2.8)	0.10	0.90
Dihydroceramide (d18:0/22:0)	58.9 (55.4–102.4)	54.5 (44.9–81.7)	65.8 (52.2–83.2)	−0.08	0.50
Ceramide (d18:1/23:0)	8.2×10^2 (7.2–11.8)$\times 10^2$	6.4×10^2 (4.9–7.4)$\times 10^2$	7.5×10^2 (6.6–8.6)$\times 10^2$	−0.08	0.08
Dihydroceramide (d18:0/23:0)	49.4 (45.3–68.3)	43.3 (35.7–61.7)	50.6 (42.7–69.5)	0.03	0.82
Ceramide (d18:1/25:0)	1.2×10^2 (1.0–1.6)$\times 10^2$	1.1×10^2 (0.8–1.1)$\times 10^2$	92.6 (82.9–118.2)	−0.20	0.20
Ceramide (d18:1/26:0)	17.8 (16.2–27.9)	16.9 (11.4–22.3)	13.2 (12.3–16.8)	−0.35	0.09
Dihydroceramide (d18:0/25:0)	3.5 (2.9–4.8)	3.3 (2.4–4.4)	3.2 (2.8–4.6)	−0.06	0.77
Dihydroceramide (d18:0/26:0)	NQ	NQ	NQ	NA	NA

DQ-disqualified.

NQ-not quantifiable.
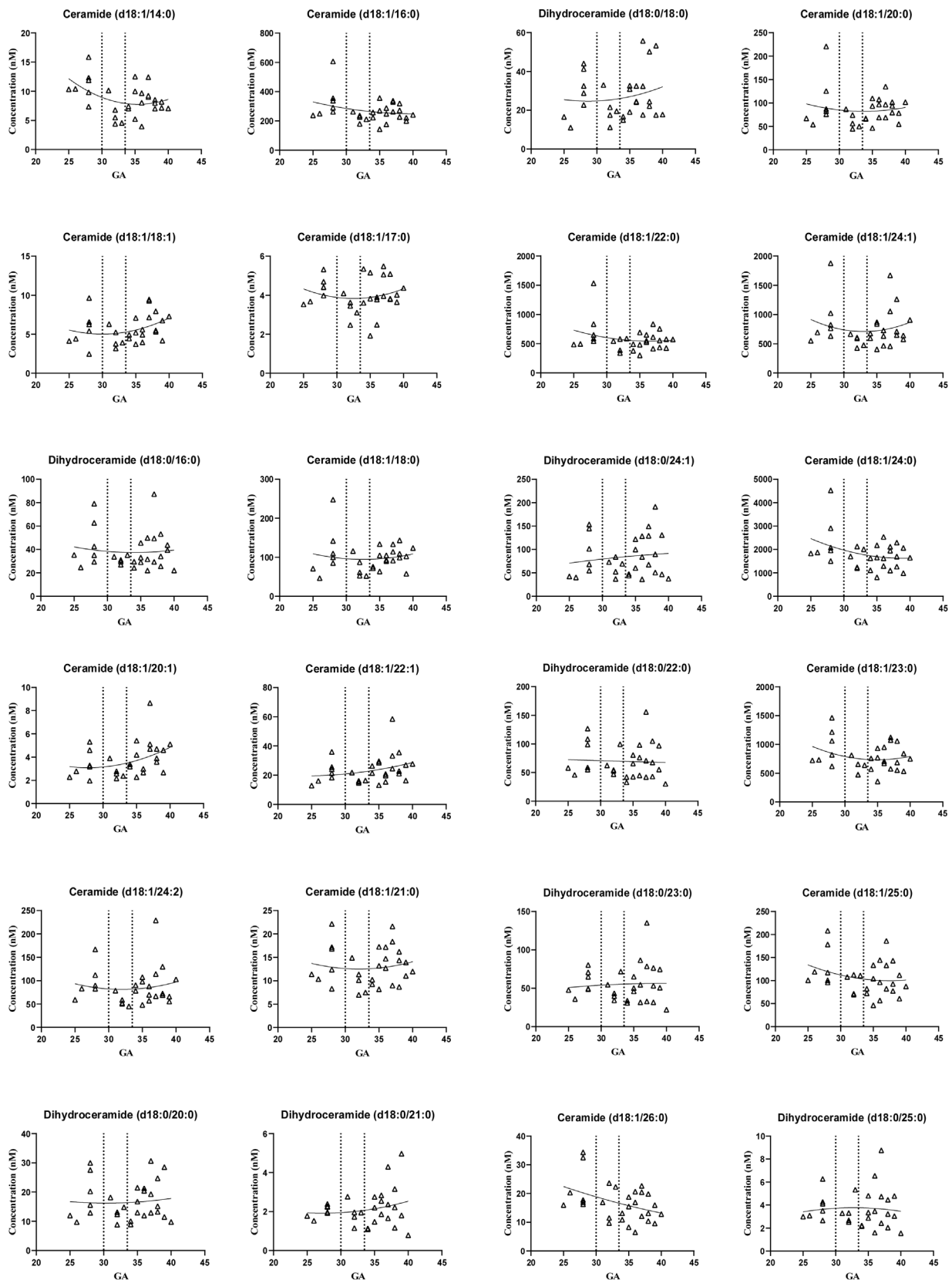
Fig. 5. Gestational age-dependent serological baseline plots of individual ceramides and dihydroceramides from normal pregnancy samples. The X-axis represents the gestational age in weeks, and the Y-axis represents the concentrations of the analyte in nM. The two dotted lines represent the 30 weeks and 34 weeks of gestation.
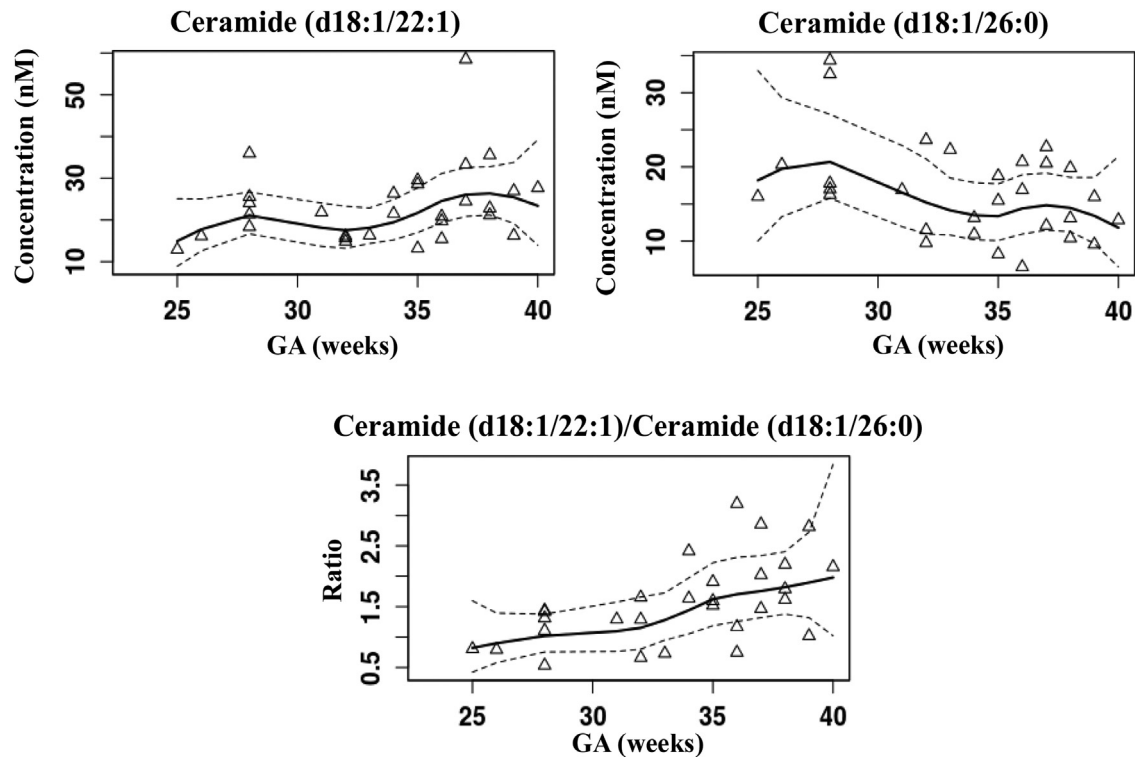
Fig. 6. Gestational age-dependent serological scatter plots of ceramide (d18:1/22:1), (d18:1/26:0), and their ratio from normal pregnancy samples. Locally estimated scatterplot smoothing (LOESS) curves (the solid lines) and 95 % confidence intervals (the dotted lines) were plotted. The smoothed value was calculated by a quadratic polynomial least-squares regression over a span of 0.75.

ranges reported by Mayo Clinic $(1.90{\sim}3.60 \times 10^2, 0.50{\sim}1.40 \times 10^2,$ and $0.65{\sim}1.65 \times 10^3$ nM for ceramides (d18:1/16:0), (d18:1/18:0), and (d18:1/24:1), respectively). Spearman correlation test identified 3 ceramides, (d18:1/20:1) (R = 0.397; P = 0.033), (d18:1/22:1) (R = 0.339; P = 0.072), and (d18:1/18:1) (R = 0.336; P = 0.074), that were strongly correlated with GA (R > 0.3) in the positive direction and 1 ceramide, (d18:1/26:0) (R=-0.346; P = 0.066), that was strongly correlated with GA (R<-0.3) in the negative direction. The regression analysis based on quadratic polynomial fitting was used to simulate the alteration of ceramide and dihydroceramide levels as a function of GA in Fig. 5. The ratios of concentrations between positively correlated ceramides and negatively correlated ceramides demonstrated stronger association with GA [ratio of ceramides (d18:1/20:1)/(d18:1/26:0) (R = 0.558; P = 0.002), ratio of ceramides (d18:1/22:1)/(d18:1/26:0) (R = 0.566; P = 0.001), and ratio of ceramides (d18:1/18:1)/(d18:1/26:0) (R = 0.458; P = 0.012)] than the use of a single ceramide. The ratios of ceramides (d18:1/20:1)/(d18:1/26:0) (P = 0.002) and ceramides (d18:1/22:1)/(d18:1/26:0) (P = 0.001) were found to be significantly changed as a function of GA by Kruskal-Wallis H-test. Owing to its stronger statistical significance and gestational correlation, the ratio of ceramides (d18:1/22:1)/(d18:1/26:0) was therefore selected as the serological marker to establish the normal pregnancy baseline from mid- to late-gestation. The gestational baseline trending of ceramide (d18:1/22:1)/ceramide (d18:1/26:0) ratio was estimated using LOESS, and a monotonic increase from 25 weeks to 40 weeks of gestation was observed (Fig. 6). In addition, the correlations between concentrations of pairwise dihydroceramide precursor and ceramide product were also evaluated by Spearman correlation test. Strong correlations (R > 0.3) were observed for ceramide (d18:1/16:0) & dihydroceramide (d18:0/16:0) (R = 0.554; P = 0.002), ceramide (d18:1/18:0) & dihydroceramide (d18:0/18:0) (R = 0.591; P = 0.001), ceramide (d18:1/20:0) & dihydroceramide (d18:0/20:0) (R = 0.442; P = 0.016),

ceramide (d18:1/22:0) & dihydroceramide (d18:0/22:0) (R = 0.346; P = 0.065), ceramide (d18:1/24:1) & dihydroceramide (d18:0/24:1) (R = 0.342; P = 0.069), and ceramide (d18:1/25:0) & dihydroceramide (d18:0/25:0) (R = 0.441; P = 0.017) pairs.

Ceramide synthases (CerS) are a family of enzymes that catalyze the biosynthesis of dihydroceramide from sphingosine during the de novo synthetic pathway of ceramide. Six isoforms of CerS have been identified in mammals, each of which seems to exert disparate specificities for the de novo synthesis of ceramides with distinct lengths of acyl chains [25]. Although they are known to share homology on the catalytic mechanism, enzymatic structure, and cytoplasmic localization, recent studies have suggested that different CerS isoforms play distinctive roles in various biological processes, such as cell proliferation and differentiation [25]. Our results illustrated that a) medium-chain ceramides that are synthesized by CerS5 and CerS6, including ceramides (d18:1/14:0) (R=-0.287) and (d18:1/16:0) (R=-0.164), were negatively correlated with GA; b) long-chain ceramides that are synthesized by CerS1, CerS2, and Cer4, including ceramides (d18:1/18:1) (R = 0.336), (d18:1/20:1) (R = 0.396), (d18:1/22:1) (R = 0.339), (d18:1/18:0) (R = 0.223), and (d18:1/20:0) (R = 0.194), were positively correlated with GA; c) very long-chain ceramides that are synthesized by CerS2 and CerS3, including ceramide (d18:1/24:0) (R=-0.210), ceramide (d18:1/25:0) (R=-0.196), and ceramide (d18:1/26:0) (R=-0.346), were negatively correlated with GA. These findings collectively revealed the marked differences on the cellular behavior and catalytic activity of various CerS isoforms from mid- to late-gestation during the development of normal pregnancy, implying their differential mechanistic roles in maintaining the gestational homeostasis of maternal-fetal interactions. Furthermore, we also observed positive correlation between levels of dihydroceramides and ceramides with identical acyl chain length and saturation degree in maternal circulation, which is consistent with the existing knowledge on their associations with ceramide de novo synthesis [25].

Ceramides, as metabolic messengers, are crucial mediator to the modulation of biological activities in pregnancy, which could serve as potential molecular targets to comprehensively understand the underlying pathophysiology of related disorders. Our study, for the first time, characterized 8 endogenous ceramide and dihydroceramide species with novel chemical structures and quantified their levels in human blood, with high sensitivity and specificity accomplished by our new methodology. The new species were ceramides (d18:1/17:0), (d18:1/20:1), (d18:1/21:0), (d18:1/24:2) and dihydroceramides (d18:0/18:1), (d18:0/21:0), (d18:0/23:0), (d18:0/25:0). The majority of these unusual analytes were odd-chain ceramides and dihydroceramides derived from odd-chain fatty acids, which are not endogenously produced by the human body. Dairy products and meat from ruminant animals have been suggested to be important sources of odd-chain saturated fatty acids [26]. In addition, population-based studies have identified an inverse relationship between plasma levels of odd-chain saturated fatty acids and the risk of coronary heart disease [27] and type 2 diabetes [28]. Our study hence provides evidence for the association of odd-chain ceramides with gestation and offers insights into their potentially distinctive roles in the development of normal pregnancy.

The gestational alterations of de novo synthetic ceramides seem to be associated with placental hormones such as leptin [29]. Leptin is a secreted hormone that affects the central regulation of energetic homeostasis, neuroendocrine function, and cytoplasmic metabolism. It tends to increase progressively in the first and second trimesters, peak in the third, and returns to pre-pregnancy levels prior to parturition [30]. Recent studies have shown that leptin promotes the mitochondrial lipid oxidation in both adipose and non-adipose tissues and alleviates the ectopic accumulation of lipotoxic ceramide. Although connections among malonyl-CoA, carnitine palmitoyl transferase-1c, serine palmitoyl transferase, leptin, and ceramide have been established, the underlying biology remains to be fully understood [29]. Our LC/MS/MS approach with high sensitivity and specificity might thus serve as a good practical tool to explore our understanding on the physiological roles of sphingolipids and their potential associations with placental hormones like leptin in the gestation.

Our study has several limitations. First, the sample size of the cohort was small. Second, the cohort lacked racial heterogeneity. Thus, the generalizability of the results awaits larger and more racially diverse study populations. Third, no samples were collected from the first and early second trimester. This limits the predictive utility of the baseline in early gestation.

4. Conclusion

This study presents the development and validation of a high-throughput LC/MS/MS method for simultaneous quantification of 16 ceramides and 10 dihydroceramides in human serum within 5 min by using stable isotope-labeled ceramides as ISs. Our method employs a simple protein precipitation method for sample preparation, reverse phase isocratic elusion for chromatographic separation, and MRM for mass spectrometric detection. The validated assay has been validation according to FDA guideline and utilized to determine serological baselines of ceramides and dihydroceramides in normal pregnancy across gestation. A ceramide ratio (d18:1/22:1)/(d18:1/26:0) with a unique gestational pattern was observed. In view of its high sensitivity, specificity, throughput, and low volume sample requirement, this method is expected to provide quantitative insights into the biology of sphingolipids during normal pregnancy, making it a potentially good practical approach to monitor the health status of pregnant women along gestation.

Authorship contributions

Conception and design of study: Qianyang Huang, Shiying Hao, Xiaoming Yao, Xuefeng B. Ling; Acquisition of data: Qianyang Huang, Xiao Li, Donghai Lai, Chunle Han, Jin You; Analysis and/or interpretation of data: Qianyang Huang, Shiying Hao, Xiaoming Yao, Xuefeng B. Ling.

Drafting the manuscript: Qianyang Huang, Shiying Hao, Xiaoming Yao, Xuefeng B. Ling; Revising the manuscript critically for important intellectual content: James Schilling, Kuo Yuan Hwa, Sheeno Thyparambil, John Whitin, Harvey J. Cohen, Henry Chubb, Scott R. Ceresnak, Doff B. McElhinney, Ronald J. Wong, Gary M. Shaw, David K. Stevenson, Karl G. Sylvester, Xuefeng B. Ling.

Approval of the version of the manuscript to be published (the names of all authors must be listed): Qianyang Huang, Shiying Hao, Xiaoming Yao, Jin You, Xiao Li, Donghai Lai, Chunle Han, James Schilling, Kuo Yuan Hwa, Sheeno Thyparambil, John Whitin, Harvey J. Cohen, Henry Chubb, Scott R. Ceresnak, Doff B. McElhinney, Ronald J. Wong, Gary M. Shaw, David K. Stevenson, Karl G. Sylvester, Xuefeng B. Ling.

Availability of data and materials

The datasets used and/or analyzed in this study are available upon request to the corresponding author.

Declaration of Competing Interest

The authors declare that they have no conflict of interests.

Acknowledgement

Appendix A. Supplementary data

Supplementary material related to this article can be found, in the online version, at doi:https://doi.org/10.1016/j.jpba.2020.113639.

References

[1] C.R. Gault, L.M. Obeid, Y.A. Hannun, An overview of sphingolipid metabolism: from synthesis to breakdown, Adv. Exp. Med. Biol. 688 (2010) 1–23, http://dx.doi.org/10.1007/978-1-4419-6741-1_1.

[2] D. Davis, M. Kannan, B. Wattenberg, Orm/ORMDL proteins: gate guardians and master regulators, Adv. Biol. Regul. 70 (2018) 3–18, http://dx.doi.org/10.1016/j.jbior.2018.08.002.

[3] Y.A. Hannun, L.M. Obeid, Principles of bioactive lipid signalling: lessons from sphingolipids, Nat. Rev. Mol. Cell Biol. 9 (2008) 139–150, http://dx.doi.org/10.1038/nrm2329.

[4] Y.H. Zeidan, Y.A. Hannun, Translational aspects of sphingolipid metabolism, Trends Mol. Med. 13 (2007) 327–336, http://dx.doi.org/10.1016/j.molmed.2007.06.002.

[5] N.Z. Ding, Q.R. Qi, X.W. Gu, R.J. Zuo, J. Liu, Z.M. Yang, De novo synthesis of sphingolipids is essential for decidualization in mice, Theriogenology 106 (2018) 227–236, http://dx.doi.org/10.1016/j.theriogenology.2017.09.036.

[6] M. Melland-Smith, L. Ermini, S. Chauvin, H. Craig-Barnes, A. Tagliaferro, T. Todros, M. Post, I. Caniggia, Disruption of sphingolipid metabolism augments ceramide-induced autophagy in preeclampsia, Autophagy 11 (2015) 653–669, http://dx.doi.org/10.1080/15548627.2015.1034414.

[7] X. Gao, N. Ning, B. Kong, Y. Xu, H. Xu, C. Zhou, S. Li, Y. Shao, J. Qiu, J. Li, Aberrant sphingolipid metabolism in the human fallopian tube with ectopic pregnancy, Lipids 48 (2013) 989–995, http://dx.doi.org/10.1007/s11745-013-3818-y.

[8] S. Chauvin, Y. Yinon, J. Xu, L. Ermini, J. Sallais, A. Tagliaferro, T. Todros, M. Post, I. Caniggia, Aberrant TGFbeta signalling contributes to dysregulation of sphingolipid metabolism in intrauterine growth restriction, J. Clin. Endocrinol. Metab. 100 (2015) E986–996, http://dx.doi.org/10.1210/jc.2015-1288.

[9] K. Mizugishi, T. Inoue, H. Hatayama, J. Bielawski, J.S. Pierce, Y. Sato, A. Takaori-Kondo, I. Konishi, K. Yamashita, Sphingolipid pathway regulates

innate immune responses at the fetomaternal interface during pregnancy, J. Biol. Chem. 290 (2015) 2053–2068, http://dx.doi.org/10.1074/jbc.M114.628867.

[10] M.M. Siddique, Y. Li, B. Chaurasia, V.A. Kaddai, S.A. Summers, Dihydroceramides: From bit players to lead actors, J. Biol. Chem. 290 (2015) 15371–15379, http://dx.doi.org/10.1074/jbc.R115.653204.

[11] A.Y. Lee, J.W. Lee, J.E. Kim, H.J. Mock, S. Park, S. Kim, S.H. Hong, J.Y. Kim, E.J. Park, K.S. Kang, K.P. Kim, M.H. Cho, Dihydroceramide is a key metabolite that regulates autophagy and promotes fibrosis in hepatic steatosis model, Biochem. Biophys. Res. Commun. 494 (2017) 460–469, http://dx.doi.org/10.1016/j.bbrc.2017.10.110.

[12] A. Dobierzewska, S. Soman, S.E. Illanes, A.J. Morris, Plasma cross-gestational sphingolipidomic analyses reveal potential first trimester biomarkers of preeclampsia, PLoS One 12 (2017), http://dx.doi.org/10.1371/journal.pone.0175118.

[13] K. Charkiewicz, J. Goscik, A. Blachnio-Zabielska, G. Raba, A. Sakowicz, J. Kalinka, A. Chabowski, P. Laudanski, Sphingolipids as a new factor in the pathomechanism of preeclampsia - Mass spectrometry analysis, PLoS One 12 (2017), http://dx.doi.org/10.1371/journal.pone.0177601.

[14] G. Vielhaber, L. Brade, B. Lindner, S. Pfeiffer, R. Wepf, U. Hintze, K.-P. Wittern, H. Brade, Mouse Anti-Ceramide Antiserum: a Specific Tool for the Detection of Endogenous Ceramide, 2001.

[15] H. Jiang, F.F. Hsu, M.S. Farmer, L.R. Peterson, J.E. Schaffer, D.S. Ory, X. Jiang, Development and validation of LC–MS/MS method for determination of very long acyl chain (C22:0 and C24:0) ceramides in human plasma, Anal. Bioanal. Chem. 405 (2013) 7357–7365, http://dx.doi.org/10.1007/s00216-013-7166-9.

[16] D. Kauhanen, M. Sysi-Aho, K.M. Koistinen, R. Laaksonen, J. Sinisalo, K. Ekroos, Development and validation of a high-throughput LC–MS/MS assay for routine measurement of molecular ceramides, Anal. Bioanal. Chem. 408 (2016) 3475–3483, http://dx.doi.org/10.1007/s00216-016-9425-z.

[17] CLSI, Liquid Chromatography-mass Spectrometry Methods; Approved Guideline. CLSI Document C62- a, Clinical and Laboratory Standards Institute, Wayne, PA, 2014.

[18] G. Liebisch, W. Drobnik, M. Reil, B. Trümbach, R. Arnecke, B. Olgemöller, A. Roscher, G. Schmitz, Quantitative Measurement of Different Ceramide Species From Crude Cellular Extracts by Electrospray Ionization Tandem Mass Spectrometry (ESI-MS/MS), 1999 www.jlr.org.

[19] X. Han, Characterization and direct quantitation of ceramide molecular species from lipid extracts of biological samples by electrospray ionization tandem mass spectrometry, Anal. Biochem. 302 (2002) 199–212, http://dx.doi.org/10.1006/abio.2001.5536.

[20] Q. Huang, X. Zhou, D. Liu, B. Xin, K. Cechner, H. Wang, A. Zhou, A new liquid chromatography/tandem mass spectrometry method for quantification of gangliosides in human plasma, Anal. Biochem. 455 (2014) 26–34, http://dx.doi.org/10.1016/j.ab.2014.03.014.

[21] Q. Huang, D. Liu, B. Xin, K. Cechner, X. Zhou, H. Wang, A. Zhou, Quantification of monosialogangliosides in human plasma through chemical derivatization for signal enhancement in LC-ESI-MS, Anal. Chim. Acta 929 (2016) 31–38, http://dx.doi.org/10.1016/j.aca.2016.04.043.

[22] K. Yang, Z. Zhao, R.W. Gross, X. Han, Systematic analysis of choline-containing phospholipids using multi-dimensional mass spectrometry-based shotgun lipidomics, J. Chromatogr. B Analyt. Technol. Biomed. Life Sci. 877 (2009) 2924–2936, http://dx.doi.org/10.1016/j.jchromb.2009.01.016.

[23] US Department of Health and Human Services, Food and Drug Administration, Center for Drug Evaluation and Research and Center for Veterinary Medicine.Guidance for Industry: Bioanalytical Method Validation, 2018.

[24] C, G.U. Munar Ada, Frazee, Quantification of dehydroepiandrosterone, 11-deoxycortisol, 17-hydroxyprogesterone, and testosterone by liquid chromatography-tandem mass spectrometry (LC/MS/MS), in: U. Garg (Ed.), Clinical Applications of Mass Spectrometry in Biomolecular Analysis: Methods and Protocols, Springer, New York, New York, NY, 2016, pp. 273–279, http://dx.doi.org/10.1007/978-1-4939-3182-8_29.

[25] M. Levy, A.H. Futerman, Mammalian ceramide synthases, IUBMB Life 62 (2010) 347–356, http://dx.doi.org/10.1002/iub.319.

[26] B. Jenkins, J.A. West, A. Koulman, A review of odd-chain fatty acid metabolism and the role of pentadecanoic acid (C15:0) and heptadecanoic acid (C17:0) in health and disease, Molecules 20 (2015) 2425–2444, http://dx.doi.org/10.3390/molecules20022425.

[27] K.T. Khaw, M.D. Friesen, E. Riboli, R. Luben, N. Wareham, Plasma phospholipid fatty acid concentration and incident coronary heart disease in men and women: the EPIC-Norfolk prospective study, PLoS Med. 9 (2012), http://dx.doi.org/10.1371/journal.pmed.1001255.

[28] N.G. Forouhi, A. Koulman, S.J. Sharp, F. Imamura, J. Kröger, M.B. Schulze, F.L. Crowe, J.M. Huerta, M. Guevara, J.W.J. Beulens, G.J. van Woudenbergh, L. Wang, K. Summerhill, J.L. Griffin, E.J.M. Feskens, P. Amiano, H. Boeing, F. Clavel-Chapelon, L. Dartois, G. Fagherazzi, P.W. Franks, C. Gonzalez, M.U. Jakobsen, R. Kaaks, T.J. Key, K.T. Khaw, T. Kühn, A. Mattiello, P.M. Nilsson, K. Overvad, V. Pala, D. Palli, J.R. Quirós, O. Rolandsson, N. Roswall, C. Sacerdote, M.J. Sánchez, N. Slimani, A.M.W. Spijkerman, A. Tjonneland, M.J. Tormo, R. Tumino, D.L. van der A, Y.T. van der Schouw, C. Langenberg, E. Riboli, N.J. Wareham, Differences in the prospective association between individual plasma phospholipid saturated fatty acids and incident type 2 diabetes: the EPIC-InterAct case-cohort study, Lancet Diabetes Endocrinol. 2 (2014) 810–818, http://dx.doi.org/10.1016/S2213-8587(14)70146-9.

[29] E. Bonzon-Kulichenko, D. Schwudke, N. Gallardo, E. Molto, T. Fernandez-Agullo, A. Shevchenko, A. Andres, Central leptin regulates total ceramide content and sterol regulatory element binding protein-1C proteolytic maturation in rat white adipose tissue, Endocrinology 150 (2009) 169–178, http://dx.doi.org/10.1210/en.2008-0505.

[30] M.C. Henson, V.D. Castracane, Leptin in pregnancy: an update, Biol. Reprod. 74 (2006) 218–229, http://dx.doi.org/10.1095/biolreprod.105.045120.